International Journal of Multidisciplinary and Current Research ISSN: 2321-3124
Research Article Available at: http://ijmcr.com

Investigation of effect of B-H curve, disc material, number of electromagnet and disc on MR brake performance

Prashant Sinha[*1]

[1]Department of Mechanical Engineering, IITM, Jodhpur India

Received 26 Dec 2022, Accepted 26 Jan 2023, Available online 29 Jan 2023, **Vol.11 (Jan/Feb 2023 issue)**

Abstract

Due to the mechanical contact between the brake pad and disc material in automobile disc brakes, the lining materials are subjected to considerable frictional heat and wear. By substituting conventional disc brakes with Magnetorheological brakes, these disadvantages can be eliminated (MRB). Also, a single-disc MR brake cannot produce the necessary torque for real-world automotive applications. To counteract these drawbacks, a new multidisc MR brake design was developed. A FEM analysis of a low-carbon steel single-disc MR brake with a central electromagnet was performed without the incorporation of a B-H curve. The B-H curve was then incorporated into the analysis to examine the effect of magnetic saturation. To investigate the effect of disc material on magnetic flux, the disc material was changed from low carbon steel to iron, whose relative permeability is greater. Using three electromagnets as opposed to a single electromagnet, the effect of the number of electromagnets on the magnetic field was investigated. In order to determine the effect of disc count, a finite element analysis of a multidisc (18 disc) MR brake was conducted. FEM results conclude that the performance of a single-disc MR brake can be improved by incorporating the B-H curve and increasing the number of electromagnets from one to three. Using a multidisc brake instead of a single disc in the MR brake can also increase torque. In previous research, the effect of more than one electromagnet, the insertion of a B-H curve, and the use of multiple discs were not investigated in detail. In the present study, a detailed and schematic analysis of these factors is performed using finite element analysis, and the results are validated using an experimental MR brake setup.

Keywords: *B-H Curve, Finite Element Analysis, Single And Three Electromagnet, Single and Multi-Disc, Torque*

1. Introduction

Slow response, fluctuating torque, heavy and complex parts, braking noise due to metal-to-metal contact, and performance degradation at high speed and temperature are characteristics of automotive disc brakes [1-2]. Reduced response time, ultra-low wear, compactness, and pollution-free environment (absence of wear debris) make MR brakes a desirable alternative to conventional automotive disc brakes [3-7]. The wear of materials is the major concerned in various industries [8-25]. In the absence of a magnetic field, the carbonyl iron particle is in Brownian motion in the carrier fluid; when a magnetic field is applied, the viscosity of the MR fluid changes by 100 to 1000 times, and the carbonyl iron particle is aligned in the direction of the magnetic field and provides shear resistance [26-27] as depicted in Fig. 1. (a).

Iron particles are suspended in a carrier fluid with a surfactant to create MR fluid. Shown in Fig. 1 (b), magnetorheological brake consists of rotating cylindrical discs immersed in MR fluid and encased in an electromagnet casing.

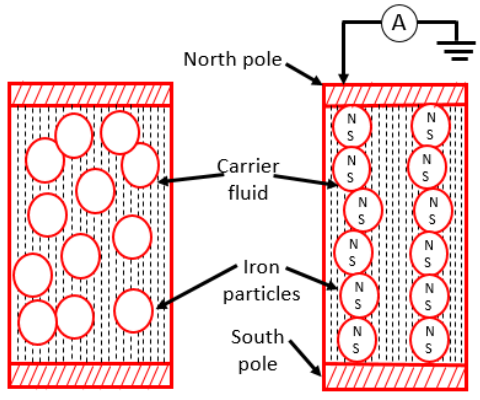

Brownian motion of iron particles without the application of magnetic field

Chain formation of iron particles with application of magnetic field

*Corresponding author's ORCID ID: 0000-0000-0000-0000
DOI: https://doi.org/10.14741/ijmcr/v.11.1.11

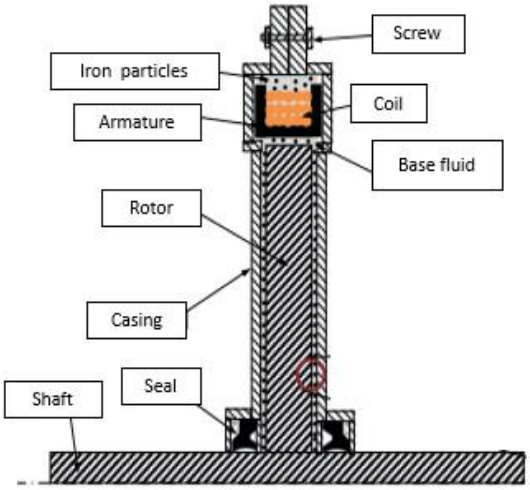

Figure 1. (a) Principle of MR fluid (b) MR brake

This figure also describes the various MR brake components. The design of the MR brake should be such that the viscosity of the MR fluid can be altered during braking in the presence of a magnetic field and vice versa; consequently, an electromagnet is used to control the braking performance of the MR brake by magnetizing the MR fluid.

Multiple studies have documented the modeling of the MR brake in order to attain maximum torque along with tribology [28-46]. Park *et al*. [48] described the tuning of MR brake to improve its performance. Sumukha *et al*. [49] optimized the casing thickness of the MR brake in order to enhance its braking performance. Karakoc *et al*. [50] utilized COMSOL software to do a finite element simulation taking into account numerous factors. To maximize the braking torque, they optimized the magnetic circuit design and many parameters including material, sealing, working area, current density, and MR fluid. Shiao and Nguyen [51] devised a multipole MR brake with several electromagnetic poles encircled by multiple coils, and they found a notable improvement in braking performance. Liu *et al*. [52] presented the best actuator dimensions using finite element analysis. Suzuki *et al*. [53] created a shear-type compact MR brake (SCMRB), and the results are compared to previous research. Li *et al*. [54] built a high-efficiency electromagnet utilizing finite element analysis and showed that braking torque increases as magnetic field strength increases. Arlak *et al*. [55] performed CFD research in order to optimize the design parameters for MR damper. Kikuchi *et al*. [56] published guidelines for the design of the form and position of MR braking yokes in order to obtain maximum torque. Sukhwani *et al*. [57] examined the influence of MR fluid gap on MR braking performance in order to determine the optimal gap thickness at which maximum torque is generated. Hongyun *et al*. [58] compared the shear yield stress of MR fluid with the compressive and tensile performance of MR fluid under different magnetic fields. Hybrid materials were developed to improve the performance of various automotive parts that were previously restricted to common materials [59-67].

It has been noted in the literature that the magnetic field depends on the magnetic permeability of the disc material. Greater torque may be generated when the magnetic permeability of the disc material is increased. Also, in our prior investigation, we discovered that MR fluid saturates after a particular magnetic field, leading to torque saturation. Therefore, FEM simulation of multidisc MR brakes may be utilized to solve this issue. Also, manual insertion of the B-H curve into the analysis is essential for the uniform creation of the magnetic field. Due to restricted shear stress, the literature indicates that a single disc MR brake cannot provide sufficient torque to replace a standard automated disc brake.

2. Finite element modelling

ANSYS software was used to model Magnetorheological Brake utilizing finite elements. A two-dimensional axi-symmetrical model has been designed to save computing time and expense. The geometry of the MR brake was created using a two-dimensional quadrilateral linked field solid element PLANE13 with four nodes (each node having four Degrees of Freedom). The element PLANE 13 can be ascribed nonlinear magnetic characteristics (B-H curves). The SI units were specified with the EMUNIT command. The (free-space permeability) value was maintained equal to $4\Pi*10^{-7}$ henries/meter. Since the MR brake disc was mounted to the rotating shaft, the spinning shaft and disc were analyzed as a single element in FEM. The magnetic flux density was determined for a particular electromagnetic coil current density. In the study, there was assumed to be no leakage of MR fluid from the casing to the environment, hence the magnetic flux on the casing borders was confined to be parallel. To impose this requirement, the constraint of parallel magnetic flux on housing borders (AZ=0) was applied. ANSYS utilizes the flux normal to all external faces by default. Using the MAGSOLV command, a 2D magnetic static analysis was done to determine the distribution of magnetic flux within the brake housing. Nonlinear analysis (using NSUBST) was carried out to accommodate a nonlinear B-H curve. During each equilibrium iteration of a nonlinear electromagnetic analysis, ANSYS computes convergence norms with accompanying convergence criteria. When defined convergence conditions are fulfilled, ANSYS deems a solution to have converged. Convergence testing can be based on magnetic potential, magnetic flux density, or magnetic field. MR brake components include a shaft, bearing, seal, housing,

rotating disc, MR fluid, and electromagnetic coil. The component's dimensions are provided in Table 1. Figure 2 depicts the 2-D modeling of an MR brake with a central electromagnet and a single disc. Figure 3 depicts the 2-D modeling of an MR brake with two side electromagnets, one center electromagnet, and a single disc. Figure 4 is a two-dimensional representation of a multidisc (18 discs) MR brake with a center electromagnet. The dimensions of the different MR brake components are listed in Table 1.

Table 1. Dimensions of various components of MR brake

Components	Dimension
Disc	Inner diameter -28mm, outer diameter-88mm
MR fluid gap	1mm
Number of turns of coil	1000
Electromagnet area	Inner diameter 50mm, outer diameter 65mm
Seal	Inner diameter – 28mm, outer diameter – 32mm
Casing	Inner diameter- 130mm, outer diameter – 180mm
Shaft	27.8mm

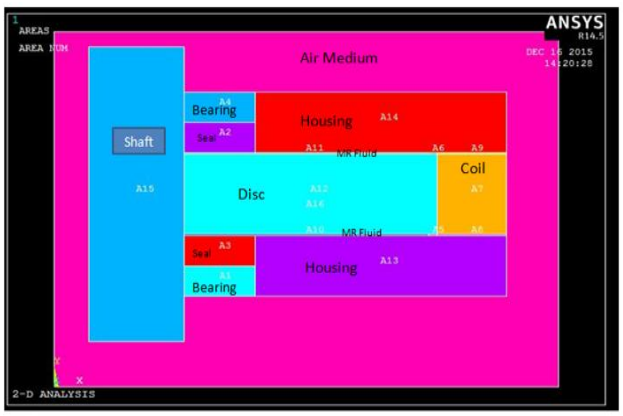

Figure 2. 2D- axisymmetric modelling of MR Brake with one central electromagnet

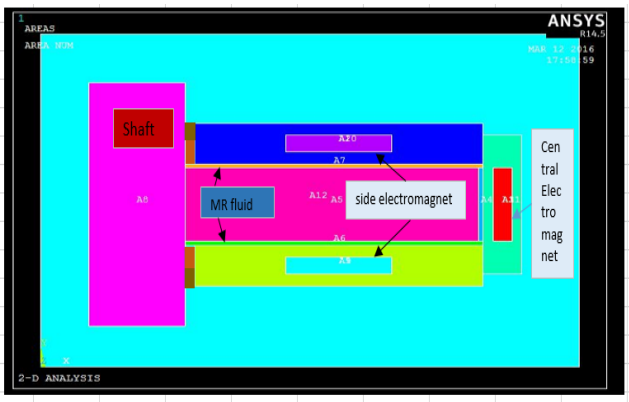

Figure 3. 2D- axisymmetric modelling of MR Brake with one central electromagnet and two sides electromagnet

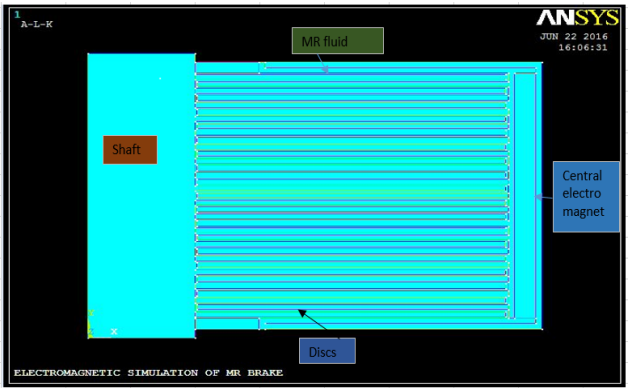

Figure 4. 2D- axisymmetric modelling of Multidisc (18 discs) MR Brake with one central electromagnet

As illustrated in Figure 5, the B-H curve is entered into the analysis using the NBUST command in order to produce a uniform magnetic flux. As various materials have varying relative permeabilities. The magnetic field produced by a material with a high permeability value is greater, and vice versa. The magnetic permeability of the material chosen for MR brake discs must be high. Table 2 lists the relative permeability values ascribed to the materials of various MR brake components.

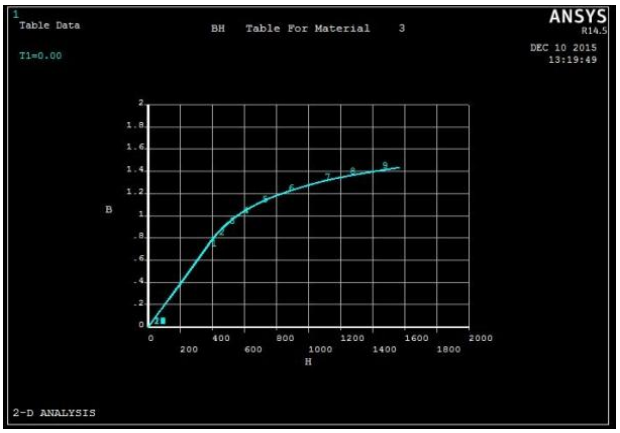

Figure 5. B-H Curve for electromagnet coil

Table 2. Relative permeability of different materials of MR brake

Parts	Material	Relative permeability
Shaft	Low carbon Steel	100
Disc	Low carbon steel/Iron 99.8% pure	100/5000
Housing	Low carbon steel	100
Seals	Natural Rubber	1
Bearing	Low carbon steel	100
MR fluid	MRF1TAH	8

3. Results and discussions

Initial analysis is done on an MR brake with a single low-carbon steel and center electromagnet. The flux lines and

vector plot in two dimensions are depicted in Figure 6(a) and Figure 6(b), respectively. The flux lines are evenly distributed across the disc's perimeter. Away from the electromagnet or near to the shaft, the dispersion of flux lines is weak and not uniform. The vector plot depicts the magnetic flux produced by a certain current. With a single low-carbon steel and central electromagnet, approximately 0.93 tesla of magnetic flux is created. From this magnetic flux density, the shear stress at various magnetic flux densities may be computed, as well as the braking torque. In the study, red indicates the largest value of magnetic flux density, while blue indicates the minimum value of magnetic flux density. The magnetic flux value is greatest near the shaft and disc's perimeter, resulting in an increase in shear stress in that specific location.

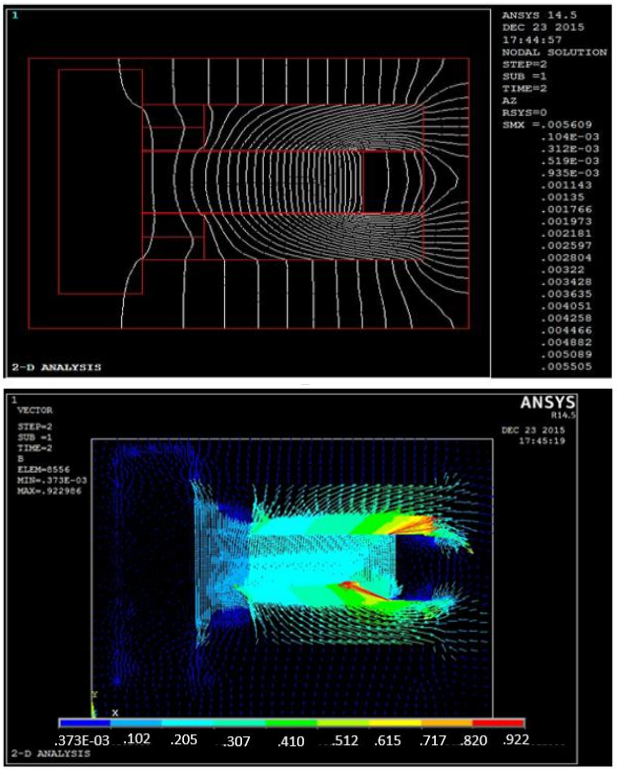

Figure 6 (a) 2D flux lines (b) Vector plot of MR brake with one central electromagnet having low carbon steel disc and without B-H curve

In order to examine the impact of magnetic saturation, a B-H curve is introduced for the same MR brake with a low carbon steel disc and central electromagnet. When a specific magnetic field strength is applied to MR fluid, the fluid will saturate. Therefore, it is preferable to use the B-H curve in analysis. As demonstrated in Figure 7, more uniform distribution is produced by integrating the B-H curve (a). However, magnetic flux lines also flow through the shaft, which increases the power loss in steady state. Figure 7(b) depicts the vector plot of the MR brake after the B-H curve was incorporated into the analysis. This graph indicates that the largest magnetic flux is created closer to the shaft, which is advantageous for braking. Also, the magnetic flux created under on-state conditions is greater than 1.03 tesla, which is greater than the magnetic flux generated without the B-H curve.

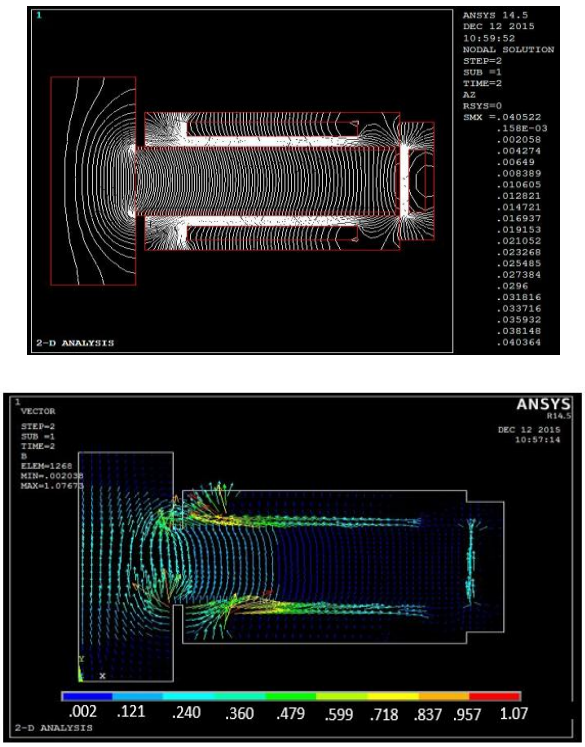

Figure 7 (a) 2D flux lines (b) Vector plot of MR brake with one central electromagnet having low carbon steel disc and with B-H curve

The above research confirms that B-H curve inclusion increases magnetic flux production. As magnetic field intensity is directly proportional to the relative permeability of the material, magnetic field production increases as the relative permeability of the material increases. To explore the influence of disc material, iron is substituted for low carbon steel since iron has a higher relative permeability value (500) than low carbon steel (100). As demonstrated in Figure 8, the formation of flux lines is more consistent when the disc material is changed from low-carbon steel to iron (Figure 8(a)). Iron as a disc material generates more magnetic flux about 1.45 Tesla than low carbon steel. In addition, as illustrated in Figure 8(b), the largest value of magnetic flux created is close to the shaft.

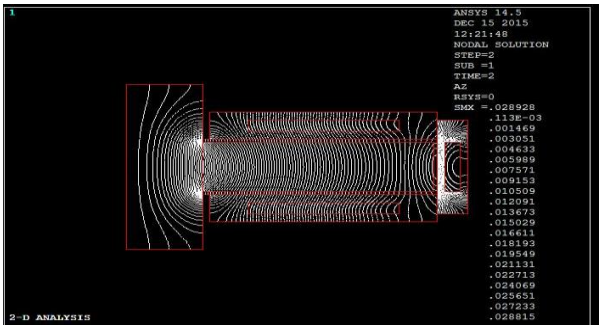

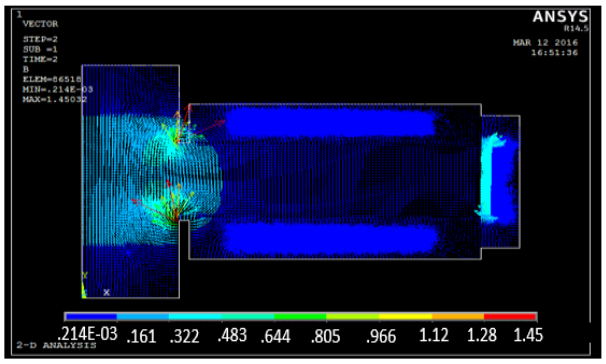

Figure 8 (a) 2D flux lines (b) Vector plot of MR with one central electromagnet having the iron disc and with B-H curve

From the above research, it is clear that an MR brake with an iron disc and a B-H curve will create higher magnetic flux. To examine the influence of the number of electromagnets, an MR brake with three electromagnets (two on the sides and one in the middle) was utilized. As seen in Figure 10, magnetic flux lines also flow through the shaft in this instance, resulting in increased power loss in the on condition (Figure10 (a)). With one central electromagnet and two side electromagnets, the total number of turns is greater, resulting in more magnetic flux generation, as magnetic flux intensity is directly proportional to the number of coil turns. As illustrated in Figure 10(b), the magnetic flux density increases around 3.44 tesla as the number of coils increases.

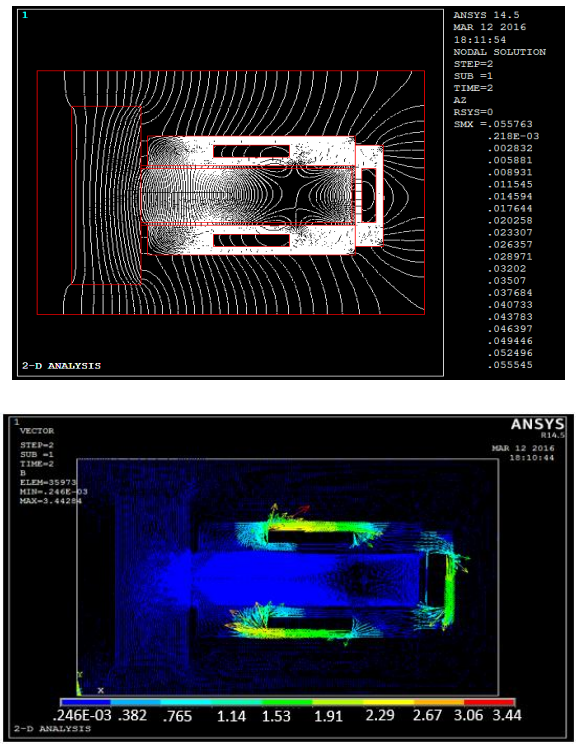

Figure 9 (a) 2D flux lines (b) Vector plot of MR with one central electromagnet and two side electromagnet having the iron disc and with B-H curve

By increasing the number of discs, more magnetic flux may be created. In order to test the equation and further improve the magnetic flux value, single discs are substituted by multidiscs (18 disc). In addition, a central electromagnet to minimize the flux around the shaft while the machine is not in operation. The size of each disc in a multidisc MR brake is 1/18 that of a single disc, ensuring that the total size of the MR brake remains unchanged and small. Also necessary for comparison with a single-disc MR brake is the same size multidisc MR brake. Other parts and dimensions of the MR brake remain unchanged. The material of the disc is maintained as iron, and the B-H curve is also incorporated into the study, since it has been determined from prior analysis that greater magnetic flux can be created by using the B-H curve and using iron as the disc material. After analysis, the 2-D flux lines are shown in Figure 10 (a). From this diagram, it is clear that no flux lines flow through the shaft; hence, in the case of multidisc MR brakes, power loss in the on state may be minimized. As demonstrated in Figure 10(b), the multidisc MR brake generates more magnetic flux about 8.96 tesla than the single disc MR brake.

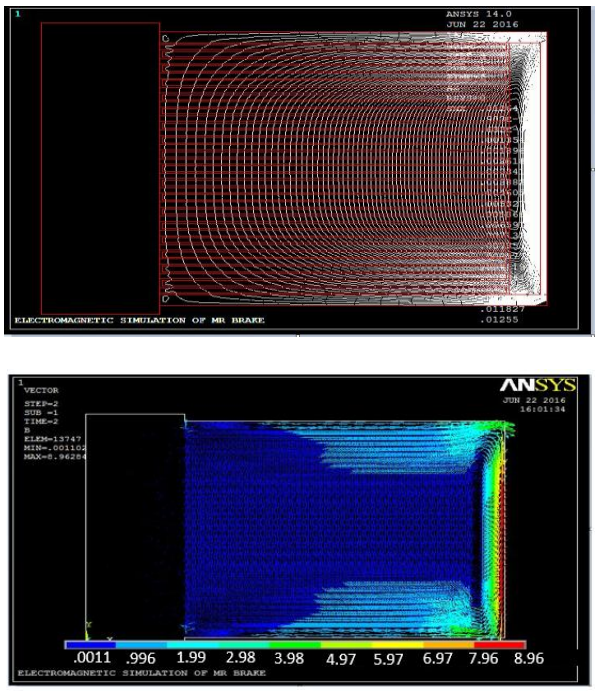

Figure 10 (a) 2D flux lines (b) Vector plot of MR with one central electromagnet having iron disc (18 disc) and with B-H curve

As illustrated in Figure 11, the torque value is also estimated for the aforementioned FEM and experimental analyses. Table 3 displays the shorthand for graphing torque versus current for. Due to the iron material's high magnetic permeability, MR brakes with iron as the disc material are able to create higher torque than MR brakes with low carbon steel as the disc material (Figure 11). After adding the B-H curve for the electromagnet coil,

additional magnetic field is created, as seen in this diagram. The multidisc MR brake (18 disc) may generate more torque at a greater distance than the single disc MR brake. Consequently, multidisc MR brakes are more effective than single disc MR brakes. Moreover, it can be shown that experimental results correspond to FEM analysis.

Table 3. Abbreviation for plotting graph (Torque vs Current)

Abbreviation	Full Form
OCE-LCS-WOBH	One central electromagnet, low carbon steel single disc, without B- H curve
OCE-LCS-WBH	One central electromagnet, low carbon steel single disc, with B- H curve
OCE-I-WBH	One central electromagnet, iron single disc, without B- H curve
OCE-TSE-I-WBH	One central electromagnet, two side electromagnet, iron single disc, with B- H curve
OCE-MDMRB-I-WBH	One central electromagnet, iron multidisc MR brake, with B- H curve

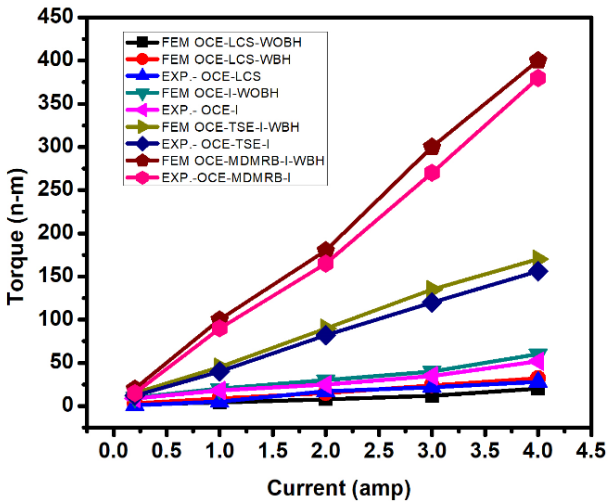

Figure 11 Torque vs current

Conclusions

Following conclusion is drawn from the FEM and experimental study

1) Incorporation of B- H curve to electromagnet, the MR brake generates more torque irrespective of any magnetic material of disc.
2) MR brake having iron disc is able to generate more torque as compared to low carbon steel as iron material has high value of relative permeability.
3) MR brake with one central electromagnet and two central electromagnet generates more torque as compared to MR brake having only one central electromagnet.
4) Multidisc MR brake is able to generate more torque leads to generation of higher friction and more shear stress which is required for braking action. Also power loss can be minimised by having multidisc MR brake as flux lines is not passing through the shaft.

References

[1]. Park, E. J., da Luz, L. F., & Suleman, A. (2008). Multidisciplinary design optimization of an automotive magnetorheological brake design. *Computers & Structures*, *86*(3-5), 207-216.
[2]. Sohn, J. W., Jeon, J., Nguyen, Q. H., & Choi, S. B. (2015). Optimal design of disc-type magneto-rheological brake for mid-sized motorcycle: experimental evaluation. *Smart Materials and Structures*, *24*(8), 085009.
[3]. Lijesh, K. P., Kumar, D., & Hirani, H. (2017). Effect of disc hardness on MR brake performance. Engineering Failure Analysis, 74, 228-238.
[4]. A. Poznic, A. Zelic, I. Szabo, Magnetorheological fluid brake basic performances testing with magnetic field efficiency improvement proposal, Hung. J. Ind. Chem. 40 (2) (2012) 113–119.
[5]. Lijesh, K. P., Kumar, D., & Gangadharan, K. V. (2018). Design of magneto-rheological brake for optimum dimension. Journal of the Brazilian Society of Mechanical Sciences and Engineering, 40(3), 1-12.
[6]. K. Karakoc, E.J. Park, A. Suleman, Design considerations for an automotive magnetorheological brake, Mechatronics 18 (8) (2008) 434–447.
[7]. Lijesh, K. P., Kumar, D., & Hirani, H. (2017). Synthesis and field dependent shear stress evaluation of stable MR fluid for brake application. Industrial Lubrication and Tribology.
[8]. Kumar, D., Harmain, G. A., Gaurav, G., Lijesh, K. P., Kuriachen, B., Hirani, H., & Philip, J. T. (2022). A Novel Seal Design to Enhance MR Brake Performance. Transactions of the Indian Institute of Metals, 1-8.
[9]. Rai, H., Thakur, D., Kumar, D., Pitkar, A., Ye, Z., Balakrishnan, V., & Gosvami, N. N. (2022). Spatial variation in nanoscale wear behavior of chemical vapor deposited monolayer WS2. Applied Surface Science, 605, 154783.
[10]. T. Philip, J., Kuriachen, B., Kumar, D., & Mathew, J. (2022). Tribo-behavioural transition of Ti6Al4V as a function of sliding velocity and load under dry sliding conditions. Tribology-Materials, Surfaces & Interfaces, 1-20.
[11]. Kumar, P., Philip, J. T., Wani, M. F., Rai, H., Vashishtha, H., Kuriachen, B., & Kumar, D. (2022). Study of Tribological Properties of EN8 Steel against Inconel X-750 Alloy under Dry and Lubricated Conditions. Transactions of the Indian Institute of Metals, 1-9.
[12]. Singh, V. P., Kumar, D., Mahto, R. P., & Kuriachen, B. (2022). Microstructural and Mechanical Behavior of Friction-Stir-Welded AA6061-T6 and AZ31 Alloys with Improved Electrochemical Corrosion. *Journal of Materials Engineering and Performance*, 1-20.
[13]. Thasleem, P., Kumar, D., Joy, M. L., & Kuriachen, B. (2022). Effect of heat treatment and electric discharge alloying on the lubricated tribology of Al–Si alloy fabricated by selective laser melting. Wear, 494, 204244.
[14]. Kumar, D., Jain, J., & Gosvami, N. N. (2022). Macroscale to nanoscale tribology of magnesium-based alloys: a review. Tribology Letters, 70(1), 1-29.
[15]. Patel, S. K., Singh, V. P., Kumar, D., Roy, B. S., & Kuriachen, B. (2022). Microstructural, mechanical and wear behavior of A7075 surface composite reinforced with WC nanoparticle through friction stir processing. Materials Science and Engineering: B, 276, 115476.

[16]. Sreesha, R. B., Chandraker, S., & Kumar, D. (2022). Optimization of tribological parameters to enhance wear and friction properties of Ti6Al4V alloy using Taguchi method. Proceedings of the Institution of Mechanical Engineers, Part J: Journal of Engineering Tribology, 13506501211062540.

[17]. Kumar, D., Gosvami, N. N., & Jain, J. (2021). Influence of temperature on crystallographic orientation induced anisotropy of microscopic wear in an AZ91 Mg alloy. Tribology International, 163, 107159.

[18]. Vashishtha, H., Kumar, D., Neelakantan, S., & Jain, J. (2021). Nano-scale superelastic response of laser-welded NiTi shape-memory alloys. Philosophical Magazine Letters, 101(10), 408-416.

[19]. Mohapatra, S., Kumar, D., Prasad, R., & Jain, J. (2021). Influence of strain path change on static recrystallisation behaviour of an extruded pure magnesium. Philosophical Magazine, 101(11), 1364-1379.

[20]. Sreesha, R. B., Kumar, D., Chandraker, S., & Agrawal, A. (2021, May). Room temperature sliding wear behavior of Ti6Al4V: A review. In AIP Conference Proceedings (Vol. 2341, No. 1, p. 040041). AIP Publishing LLC.

[21]. Thasleem, P., Kuriachen, B., Kumar, D., Ahmed, A., & Joy, M. L. (2021). Effect of heat treatment and electric discharge alloying on the tribological performance of selective laser melted AlSi10Mg. Journal of Tribology, 143(5).

[22]. Kumar, D., Jaishri, B., Meena, D. K., Huang, E. W., Chang, Y. J., Yeh, A. C., ... & Gosvami, N. N. (2021). Reversal of favorable microstructure under plastic ploughing vs. interfacial shear induced wear in aged Co1. 5CrFeNi1. 5Ti0. 5 high-entropy alloy. Wear, 468, 203595.

[23]. Philip, J. T., Kumar, D., Mathew, J., & Kuriachen, B. (2021). Tribological investigations of wear resistant layers developed through EDA and WEDA techniques on Ti6Al4V surfaces: Part II–High temperature. Wear, 466, 203540.

[24]. Kumar, D. (2021). Micro and nano-scale tribology of Mg-9Al1Zn magnesium alloy under dry and lubricated conditions (Doctoral dissertation, IIT Delhi).

[25]. Philip, J. T., Kumar, D., Mathew, J., & Kuriachen, B. (2020). Tribological investigations of wear resistant layers developed through EDA and WEDA techniques on Ti6Al4V surfaces: part I–ambient temperature. Wear, 458, 203409.

[26]. Kumbhar, B. K., Patil, S. R., & Sawant, S. M. (2015). Synthesis and characterization of magneto-rheological (MR) fluids for MR brake application. *Engineering Science and Technology, an International Journal*, *18*(3), 432-438.

[27]. Jun, J. B., Uhm, S. Y., Ryu, J. H., & Suh, K. D. (2005). Synthesis and characterization of monodisperse magnetic composite particles for magnetorheological fluid materials. *Colloids and Surfaces A: Physicochemical and Engineering Aspects*, *260*(1-3), 157-164.

[28]. Kumar, D., Jain, J., & Gosvami, N. N. (2020). Nanometer-thick base oil tribofilms with acrylamide additive as lubricants for AZ91 Mg alloy. ACS Applied Nano Materials, 3(10), 10551-10559.

[29]. Kumar, D., Gosvami, N. N., & Jain, J. (2020). Influence of crystallographic orientation on nanoscale friction and wear mechanisms of the AZ91 alloy. Tribology Letters, 68(3), 1-10.

[30]. Kumar, D., Jain, J., & Gosvami, N. N. (2020). In situ study of role of microstructure on antiwear tribofilm formation on AZ91 magnesium alloy under zinc dialkyldithiophosphate containing lubricant. Advanced Engineering Materials, 22(8), 2000335.

[31]. Philip, J. T., Kumar, D., Mathew, J., & Kuriachen, B. (2020). Experimental investigations on the tribological performance of electric discharge alloyed Ti–6Al–4V at 200–600° C. Journal of Tribology, 142(6), 061702.

[32]. Kumar, D., Goel, S., Gosvami, N. N., & Jain, J. (2020). Towards an improved understanding of plasticity, friction and wear mechanisms in precipitate containing AZ91 Mg alloy. Materialia, 10, 100640.

[33]. Philip, J. T., Kumar, D., Joshi, S. N., Mathew, J., & Kuriachen, B. (2019). Monitoring of EDM parameters to develop tribo-adaptive Ti6Al4V surfaces through accretion of alloyed matrix. Industrial Lubrication and Tribology.

[34]. Philip, J. T., Kumar, D., Mathew, J., & Kuriachen, B. (2019). Wear characteristic evaluation of electrical discharge machined Ti6Al4V surfaces at dry sliding conditions. Transactions of the Indian Institute of Metals, 72(10), 2839-2849.

[35]. Philip, J. T., Kumar, D., Mathew, J., & Kuriachen, B. (2019, September). Sliding behavior of secondary phase SiC embedded alloyed layer doped Ti6Al4V surfaces ensuing electro discharge machining. In International Conference on Advanced Surface Enhancement (pp. 163-172). Springer, Singapore.

[36]. Kumar, D., Lijesh, K. P., & Basil, K. P. (2019, August). Investigation on the impact of electrical discharge machining on the tribological properties of aluminum. In AIP Conference Proceedings (Vol. 2142, No. 1, p. 140010). AIP Publishing LLC.

[37]. Kumar, D., Lal, B., Wani, M. F., Philip, J. T., & Kuriachen, B. (2019). Dry sliding wear behaviour of Ti–6Al–4V pin against SS316L disc in vacuum condition at high temperature. Tribology-Materials, Surfaces & Interfaces, 13(3), 182-189.

[38]. Kumar, D., Jain, J., & Gosvami, N. N. (2019). Anisotropy in nanoscale friction and wear of precipitate containing AZ91 magnesium alloy. Tribology Letters, 67(2), 1-8.

[39]. Kumar, D. (2019). A Comparison between Full-Film and Mixed-Film Lubrication of Cold Strip Rolling. International Journal of Applied Engineering Research, 14(17), 3590-3597.

[40]. Kumar, D., & Rajabi, H. (2019). Effect of Lubrication on a Surface parameter of Strip in Cold Rolling with Oil in Water Emulsion. International Journal of Applied Engineering Research, 14(14), 3261-3267.

[41]. Kumar, D., Deepak, K. B., Muzakkir, S. M., Wani, M. F., & Lijesh, K. P. (2018). Enhancing tribological performance of Ti-6Al-4V by sliding process. Tribology-Materials, Surfaces & Interfaces, 12(3), 137-143.

[42]. Kumar, D., Lijesh, K. P., Deepak, K. B., & Kumar, S. (2018, May). Enhancing tribological performance of Ti-6Al-4V using pin on disc setup. In AIP Conference Proceedings (Vol. 1953, No. 1, p. 030108). AIP Publishing LLC.

[43]. Lijesh, K. P., Kumar, D., Muzakkir, S. M., & Hirani, H. (2018). Thermal and frictional performance evaluation of nano lubricant with multi wall carbon nano tubes (MWCNTs) as nano-additive.

[44]. Muzakkir, S. M., & Kumar, D. (2017, February). Analysis of a magnetorheological brake with a single low carbon steel disc using ANSYS. In 2017 International Conference on Innovative Mechanisms for Industry Applications (ICIMIA) (pp. 717-719). IEEE.

[45]. Kumar, D., Kumar, S., & Maurya, R. K. Modelling and Simulation of a Magnetorheological Brake with a Single Iron Disc with and without B–H curve Using ANSYS.

[46]. Lijesh, K. P., Kumar, D., & Gangadharan, K. V. Experimental Evaluation of Honey as Carrier Fluid for MR Brake Application.

[47]. Kumar, D., Kumar, S., & Maurya, R. K. Finite Element Analysis of Magnetorheological Brake having Three Electromagnet using ANSYS.
[48]. Park, E. J., da Luz, L. F., & Suleman, A. (2008). Multidisciplinary design optimization of an automotive magnetorheological brake design. *Computers & structures*, *86*(3-5), 207-216.
[49]. Sumukha M H, Sandeep R, Vivek N, Lijesh K P, Kumar H, Gangadharan KV (2017) Design and development of magneto-rheological brake for optimum casing thickness. In: International conference on innovative mechanisms for industry applications (ICIMIA), pp 704–709
[50]. K. Karakoc, E.J. Park, A. Suleman, Design considerations for an automotive magnetorheological brake, Mechatronics 18 (8) (2008) 434–447.
[51]. Shiao, Y., & Nguyen, Q. A. (2013). Development of a multi-pole magnetorheological brake. *Smart Materials and Structures*, *22*(6), 065008.
[52]. Liu, B., Li, W. H., Kosasih, P. B., & Zhang, X. Z. (2006). Development of an MR-brake-based haptic device. *Smart materials and structures*, *15*(6), 1960.
[53]. Suzuki, S., Kawase, Y., Yamaguchi, T., Hirata, K., & Okaue, Y. (2009). Dynamic response analysis of shear-type compact MR brake using finite element method. *IEEE Transactions on Magnetics*, *45*(3), 1728-1731.
[54]. Li, W. H., & Du, H. (2003). Design and experimental evaluation of a magnetorheological brake. *The International Journal of Advanced Manufacturing Technology*, *21*(7), 508-515.
[55]. Arlak, Z., Engin, T., & Çallı, İ. (2012). Optimal design of MR damper via finite element analyses of fluid dynamic and magnetic field. *Mechatronics*, *22*(6), 890-903.
[56]. Kikuchi, T., Furusho, J., Yamaguchi, Y., & Kimura, S. (2007). Design of the high-performance MR brake and its characteristics. In *Electrorheological Fluids And Magnetorheological Suspensions* (pp. 667-673).
[57]. Sukhwani, V. K., & Hirani, H. (2008). Design, development, and performance evaluation of high-speed magnetorheological brakes. *Proceedings of the Institution of Mechanical Engineers, Part L: Journal of Materials: Design and Applications*, *222*(1), 73-82.
[58]. Hongyun W, Chang B, Junwu K, Chunfu G and Wang X 2011 J. Intel. Mat. Syst. Str. 22 811-16.
[59]. Singh, V. P., & Kuriachen, B. (2022). Experimental investigations into the mechanical and metallurgical characteristics of friction stir welded AZ31 magnesium alloy. *Journal of Materials Engineering and Performance*, *31*(12), 9812-9828.
[60]. Kumar, R., Dwivedi, R. K., Singh, V. P., Kuriachen, B., & Krishnan, N. A. (2022). Influence of Toughness and Retained Austenite on Wear Behaviour of Carbide-Free Bainite in High Silicon Steel. *Transactions of the Indian Institute of Metals*, 1-10.
[61]. Ranjole, C., Singh, V. P., Kuriachen, B., & Vineesh, K. P. (2022). Numerical Prediction and Experimental Investigation of Temperature, Residual Stress and Mechanical Properties of Dissimilar Friction-Stir Welded AA5083 and AZ31 Alloys. *Arabian Journal for Science and Engineering*, 1-13.
[62]. Patel, S. K., Singh, V. P., Roy, B. S., & Kuriachen, B. (2021). Microstructural, mechanical and wear behavior of A7075 surface composite reinforced with WC and ZrSiO4 nanoparticle through friction stir processing. *Journal of Manufacturing Processes*, *71*, 85-105.
[63]. Singh, V. P., Patel, S. K., & Kuriachen, B. (2021). Mechanical and microstructural properties evolutions of various alloys welded through cooling assisted friction-stir welding: A review. *Intermetallics*, *133*, 107122.
[64]. Singh, V. P., Patel, S. K., Ranjan, A., & Kuriachen, B. (2020). Recent research progress in solid state friction-stir welding of aluminium–magnesium alloys: a critical review. *Journal of Materials Research and Technology*, *9*(3), 6217-6256.
[65]. Kumar, A., Singh, R. C., Chaudhary, R., & Singh, V. P. (2020, April). Tribological studies and microstructural characterisation of SiC and fly ash particles based aluminium 2024 alloy composites prepared through stir casting route. In *IOP Conference Series: Materials Science and Engineering* (Vol. 804, No. 1, p. 012025). IOP Publishing.
[66]. Kumar, A., Singh, R. C., & Chaudhary, R. (2022). Investigation of Microstructure and Several Quality Characteristics of AA7075/Al2O3/Coconut Shell Ash Hybrid Nano Composite Prepared through Ultrasonic Assisted Stir-Casting. *Journal of Materials Engineering and Performance*, 1-16.
[67]. Kumar, A., Singh, R. C., & Chaudhary, R. (2022). Investigation of Nano-Al2O3 and Micro-coconut Shell Ash (CSA) Reinforced AA7075 Hybrid Metal–Matrix Composite Using Two-Stage Stir Casting. *Arabian Journal for Science and Engineering*, 1-15.